Hypothesis Article:

The Pharmacological Effect and Mechanism of Lanthanum

Hydroxide on Vascular Calcification Caused by Chronic Renal

Failure Hyperphosphatemia

Lu-Lu Zhao[1, #], Sheng-Nan Wang[1, #], Hong Liu[1], Xiao-Li Du[1], Ren Bu[1],

Bing Li[1], Rui-Lan Han[1], Jie Gao[1], Yang Liu[1], Jian Hao[2], Jian-Rong Zhao[2],

Yan Meng[2], Gang Li[1*]

[1]Department of Pharmacology, College of Pharmacy, the Inner Mongolian Medical University, Jinshan Development, Hohhot, 010110, the Inner Mongolia Autonomous Region, China

[2]Department of Nephrology, The Affiliated Hospital of Inner Mongolia Medical University, Hohhot, 010050, Inner Mongolia, People's Republic of China

[#]These authors contribute equally to this work.

[*]Corresponding authors, Gang Li, Department of Pharmacology, College of Pharmacy, the Inner Mongolian Medical University, Jinshan Street, Hohhot 010110, the Inner Mongolia Autonomous Region, China

Email: cnnmligang@hotmail.com

Phone: 86-471 6653 141

Number of words:

in the Abstract: 250

in the Introduction section: 898

in the Discussion section: 1233

Total (excluding Figure legends and references): 7216

Number of figures: 10

Number of references: 38

Running title: Lanthanum hydroxide, vascular calcification

Abbreviations:

CKD, chronic kidney disease;

CVD, cardiovascular diseases;

ESRD, end-stage renal disease;

PTH, parathyroid hormone;

FGF23, fibroblast growth factor 23;

Pi, phosphorus;

Scr, serum creatinine;

BUN, serum urea nitrogen;

CT, computed tomography;

VSMCs, Human aortic smooth muscle cells;

SM22α, smooth muscle SM;

BMP-2, bone morphogenetic protein 2;

Runx2, runt-related transcription factor 2;

TRAF6, TNF receptor associated factor 6;

NF-κB, nuclear factor-κB;

LaCl$_3$, lanthanum chloride;

αSMA, α-smooth muscle actin;

CBFA1, core-binding factor α-1;

MSX2, homeobox 2;

CBFA1, transcription factor;

ALP, Alkaline phosphatase;

LPS, Lipopolysaccharide (NF-κB agonist)

ABSTRACT

Background and Purpose: To investigate the treatment and mechanism of lanthanum hydroxide on hyperphosphate-induced vascular calcification in chronic renal failure.

Experimental Approach: Develop a rat model of CKD hyperphosphatemia. Rats were randomly allocated to the model, lanthanum hydroxide, lanthanum carbonate, Calcium carbonate groups. Determination of serum biochemical indicators and the determination of pathological analysis of kidney tissue, Von Kossa staining and CT scan on the aortic vessels. The proteomic analysis of aortic tissue *in Vivo*. A calcified VSMCs model was established. The calcium content and ALP activity were measured. RT-PCR measures the mRNA expression level of SM22α, Runx2, BMP-2 and TRAF6. Western Blot measures the protein expression level of SM22α, Runx2, BMP-2, TRAF6 and NF-κB.

Key Results: Through the detection of serum biochemical indicators and pathological analysis of kidney tissue, it can be summaryed that lanthanum hydroxide has the effect of delaying the progression of renal failure and protecting renal function. We found that the administration of lanthanum hydroxide delayed the development of vascular calcification induced by hyperphosphatemia in CKD. It can be concluded that lanthanum hydroxide may affect vascular calcification through the NF-κB pathway. In cultured VSMCs, treatment with Lanthanum chloride (LaCl$_3$) blunted phosphate-induced calcification, osteo-/chondrogenic signaling, and NF-κB activation. Lanthanum hydroxide significantly reduces the expression of Runx2, BMP-2, TRAF6 and NF-κB.

Conclusion and Implications: Lanthanum hydroxide has a protective effect on the kidneys, and can delay the development of vascular calcification by reducing serum phosphorus concentration.

KEYWORDS: Lanthanum hydroxide, vascular calcification, chronic renal failure, hyperphosphatemia, pharmacological effect, mechanism

1 INTRODUCTION

Chronic kidney disease(CKD) is defined as a group of abnormalities that can affect the kidneys structure or function and are present for more than 3 months with health implications(Inker et al., 2014). According to a recent systematic analysis, the global prevalence of adult CKD in 2010 was 10.4% for men and 11.8% for women, which

was lower in developed countries and higher in low and middle-income countries(Mills et al, 2015).

Cardiovascular diseases (CVD) are the main cause of death in CKD patients. Cardiovascular diseases account for 30-50% of all-cause mortality in CKD and end-stage renal disease (ESRD) patients worldwide(Collins AJ, Foley RN, Gilbertson DT, & Chen SC, 2015; Masakane et al., 2015). Vascular Calcification is an independent risk factor leading to increased cardiovascular mortality in CKD patients. Many studies have confirmed that hyperphosphatemia can cause cardiovascular complications, such as vascular calcification and left ventricular hypertrophy, thereby increasing the risk of death from CVD in CKD patients (Block GA, Klassen PS, Lazarus JM, Ofsthun N, Lowrie EG, & Chertow GM, 2004; Briet M, & Burns KD, 2012; Smith ER, 2016; Goodman et al, 2000; Russo, 2011).

There are four types of vascular calcification: arterial intima calcification, arterial media calcification, aortic valve calcification and calcification defense. In ESRD patients, both intima and media have calcification, but arterial intimal calcification is the most common(Wang, 2001). Therefore, intimal and media calcification may be the main reason for the increased risk of cardiovascular death in patients with ESRD by 10 to 100 times(Huveneers S, Daemen MJ, & Hordijk PL, 2015). Intimal calcification and media calcification may exist simultaneously in ESRD patients, but their manifestations may be very different. Intimal calcification is confined to plaques, and the pathological changes are related to inflammatory reactions and lipid deposition. The main consequences may be plaque rupture and

acute vascular occlusion, which may lead to avascular necrosis. Media calcification, also known as Monckeberg's sclerosis, mainly causes lesions in the inner elastic layer, which is manifested by linear deposition of hydroxyapatite crystal calcium in the inner elastic layer of the arterial media. Compared with intimal calcification, there is mainly no inflammation. Of cells and lipid deposition. It mainly causes arterial stiffness and increased systolic blood pressure, leading to left ventricular hypertrophy, which in turn leads to heart failure. Studies have shown that calcification in the middle layer of arteries is an important predictor of cardiovascular death in ESRD patients(London GM, Guérin AP, Marchais SJ., Métivier F, Pannier B, & Adda H, 2003).

Among the various causes of vascular calcification in CKD patients, hyperphosphatemia is closely related to vascular calcification. The absorption and excretion of phosphorus by the intestines, renal tubules, intracellular and extracellular fluids and bones keep the serum phosphorus levels within the normal range. Among them, the kidney's filtration and absorption of phosphorus are the main factors affecting the steady state of serum phosphorus.

With the decline of kidney function and the decrease of nephron weight, in CKD stage 2-3, phosphate hormones such as parathyroid hormone (PTH) and fibroblast growth factor 23 (FGF 23) are synthesized to resist excessive phosphorus. These hormones mainly act on the proximal tubules of the kidney, by down-regulating type IIa and type IIc sodium-phosphorus transporters, thereby increasing renal phosphorus excretion and maintaining serum phosphorus levels within the normal range(Isakova et al, 2011; Tatsumi et al, 2016).However, as CKD enters the advanced stage, the kidneys

can no longer effectively filter the ingested phosphorus, which eventually leads to obvious hyperphosphatemia in CKD 4-5. Hyperphosphatemia is associated with a significant increase in the risk of vascular calcification morbidity and mortality, observed in both the general population as well as in patients with CKD(Dhingra et al, 2007; Da et al, 2015) .

According to the current research on the mechanism of vascular calcification, effective control of serum phosphorus levels has a certain protective effect on cardiovascular and kidney in patients with chronic kidney disease, especially in advanced patients. However, by controlling the intake of high-phosphorus foods and adequate dialysis, blood phosphorus levels cannot be effectively controlled within the ideal range. The use of phosphorus binders has become an important method to control phosphorus in the blood, mainly by combining with phosphorus in food to reduce phosphorus absorption. Oral phosphate binders combine with dietary phosphates in the intestines to prevent phosphorus absorption and become part of the management strategy to reduce and control serum phosphorus levels in patients with advanced CKD. Some observational research data indicate that the use of phosphate adhesives can prolong the survival time of patients undergoing hemodialysis.

In the current treatment of hyperphosphatemia binders, lanthanum drugs have obvious advantages. Trivalent cations have a high affinity with phosphorus and are easy to form poorly soluble complexes with phosphorus. They have low water solubility and are difficult to pass through the intestinal wall into the blood. It can be excreted through feces to achieve the effect of reducing phosphorus. Meanwhile,

lanthanum does not affect the absorption of fat-soluble vitamins and has no obvious

side effects. Lanthanum absorbed into the body is mainly excreted through the liver,

so it is suitable for dialysis patients. In the preliminary research of the research group,

it was found that nano-lanthanum hydroxide has a good effect of reducing phosphorus

and has a protective effect on the kidney(Ma et al, 2019). This study is to investigate the

treatment and mechanism of lanthanum hydroxide on hyperphosphate-induced

vascular calcification in chronic renal failure.

2 Materials and methods

2.1 Reagents and Antibodies

Lanthanum hydroxide（Laboratory synthesis）, Adenine （Sigma-

Aldrich，Cat.#V900471, USA）, Lanthanum carbonate（Sigma-

Aldrich，Cat.#325767 USA）, Calcium carbonate（Sigma-Aldrich，Cat.#V900138

USA）, Human aortic vascular smooth muscle cells(Shanghai Yubo Biological

Technology Co., Ltd. Cat.#C740，China), RNA Simple Total RNA Kit（Tiangen

Biochemical Technology (Beijing) Co., Ltd. Cat.#DP419, China）, ReverTra Ace

qPCR RT Kit（ToYoBo Life Science，Cat.#FSQ-101, China）, SYBR Green

Realtime PCR Master Mix（ToYoBo Life Science，Cat.#QPK-201），

Lipopolysaccharide（LPS, Sigma-Aldrich, Cat.#L4391），Lanthanum

chloride（$LaCl_3$, Sigma-Aldrich, Cat.#298182），Sodium pyrophosphate tetrabasic

decahydrate（PPI, Sigma-Aldrich, Cat.#S6422），Monoclonal Mouse anti-SM22α

(SC-53932, Santa Cruz Biotechnology, RRID: AB_1129519), Monoclonal Mouse

anti-BMP-2/4 (SC-137087, Santa Cruz Biotechnology, RRID: AB_2258985),

Monoclonal Mouse anti-Runx2 (SC-101145, Santa Cruz Biotechnology, RRID:

AB_1128251), Polyclonal Rabbit anti-β-Actin (K101527P, Solarbio), Monoclonal

Rabbit anti-TRAF6 (ab40675, Abcam, RRID: AB_778573），Monoclonal Mouse

anti-NF-κB（#6956, Cell Signaling Technology, RRID: AB_10828935），Anti-Mouse

IgG(H+L) (A23910, Abbkine), Anti-Rabbit IgG(H+L) (A23920, Abbkine), Polyclonal

Rabbit anti-Lamin A(10298-1-AP, Proteintech, RRID: RRID：AB_2296961).

2.2 Animals and Experimental Protocol

Male wistar rats, aged 6 weeks, 200-220g (SPF, Beijing Vital River Laboratory

Animal Technology Co. Ltd China) were being kept in a barrier environment, at

constant ambient temperature (21–22°C) and humidity (40–50%). All animals had

free access to tap water and their assigned diet. All rats were allowed to acclima-tize

to the conditions of the animal facility for a period of 7 days prior to the start of the

experiments.

The CKD animal model was established as previously described in Figure 1. For 1-2 weeks, the model rats were given 2% adenine gavaged at 200 mg kg^{-1} per day. For 3-4 weeks, All model rats gavaged every other day at the same concentration and dose. After 4 weeks, blood was collected from the fundus venous plexus of the rats, and serum phosphorus, creatinine, and urea nitrogen were detected to determine whether the model was successful. After the CKD model is successful, the model group is subdivided into Lanthanum hydroxide (0.4g kg^{-1}, 0.2g kg^{-1}, 0.1g kg^{-1}), lanthanum carbonate (0.3g kg^{-1}) and calcium carbonate (4.2g kg^{-1}) (n=9-12), which was gavaged

every day for 8 week. During the experimental period , rats were fed with standard chow in the control group or chow containing 1.2% phosphorus (Beijing Keao Xieli Feed Co.,Ltd.) in the CKD group. Serum phosphorus, creatinine, urea-nitrogen, PTH, FGF23 was measured at 4 and 8 weeks after treatment. All animals were sacrificed on the last day of the 12 week. One day prior to sacrifice, rat underwent a 12 h urine collection in individual metabolic cages, with free access to water and absolute diet. For sacrifice, rat were anesthetized with 50 mg kg^{-1} pentobarbital, with abdominal aorta blood sampling. The aorta was harvested from each animal and dissected for tissue analysis as follows: snap-frozen in liquid nitrogen for for Western blotting and RNA analysis, fixed in 10% phosphate-buffered formalin for histology; The right kidney of each animal was fixed in 10% phosphate-buffered formalin for histology. The femoral bone was separated, cleaned of soft tissues, fixed in 10% phosphate-

buffered formalin for histology.

2.3 Cell Culture

Human aortic smooth muscle cells (VSMCs) were grown in Dulbecco's Modified Eagle Medium(DMEM, high glucose; Gibco, Cat. #11995-065, USA) supplemented with 10% fetal bovine serum (FBS, Gibco, Cat.#10099-141, USA) and 1% Penicillin-streptomycin（Gibco, Cat.#15140122, USA）referring to as growth medium (GM). Cells were grown to confluence and used from passages 5 to 7. Media were changed every 2 days. To induce phosphate mediated calcification, GM was supplemented with inorganic phosphate (3 mmol/L referring to as calcification medium) in a form of Na_2HPO_4/NaH_2PO_4 (pH 7.4) in the presence or absence of La (15–60 μmol L^{-1} of $LaCl_3 \times 6H_2O$) for 6 days.

2.4 Serum biochemistry

Serum calcium, phosphorus, creatinine, and urea levels were measured using biochemical detection kit (Nanjing Jiancheng Bioengineering Institute,China). Urea concentration was evaluated using the Urease-GLDH method. Creatinine concentration was evaluated Sarcosine oxidase, while calcium concentration was evaluated using the MTB method. PTH ,and FGF23, were measured by a rat ELISA kit (Shanghai Yi Li Biological Technology Co.,Ltd. ，China).

2.5 Histologic analyses

Tissue samples for histological analysis were fixed in 10% phosphate-buffered

formalin . Tissues were embedded in paraffin and H&E, Von Kossa, and EVG staining

performed according to standard methods(Wuhan Saville Biotechnology Co.,Ltd.

China). Imaging of stained sections was performed using a LEICA DM 2000 (Leica

Microsystems GmbH, Wetzlar, Germany) microscope.

2.6 In vivo computed tomography (CT) analysis

To evaluate calcified areas of the aorta, rats were Rats were anesthetized by

intraperitoneal injection of 20% urethane and subjected to CT imaging using a

PET/CT (SIEMENS Inveon MM, Siemens Ltd.Germany).

2.7 TMT modified quantitative proteomics

The sample was grinded by liquid nitrogen into cell powder and then transferred to a

5-mL centrifuge tube. After that, four volumes of lysis buffer (8 M urea, 1% Protease

Inhibitor Cocktail) was added to the cell powder, followed by sonication three times

on ice using a high intensity ultrasonic processor (Scientz). The remaining debris was

removed by centrifugation at 12,000 g at 4 °C for 10 min. Finally, the supernatant was

collected and the protein concentration was determined with BCA kit according to the

manufacturer's instructions.

Take an equal amount of each sample protein for enzymatic hydrolysis, add an

appropriate amount of standard protein, and adjust the volume to the same with the

lysis buffer. Add 1 volume of pre-cooled acetone, vortex to mix, then add 4 volumes

of pre-cooled acetone, and precipitate at -20°C for 2 h. Centrifuge at 4500 g for 5 min,

discard the supernatant, and wash the precipitate twice with pre-cooled acetone. After

drying the pellet, add TEAB at a final concentration of 200 mM, ultrasonically

disperse the pellet, add trypsin at a ratio of 1:50 (protease: protein, m m^{-1}), and

hydrolyze overnight. Add dithiothreitol (DTT) to a final concentration of 5 mM, and

reduce at 56°C for 30 min. Then add iodoacetamide (IAA) to make the final

concentration 11 mM, and incubate for 15 min at room temperature in the dark.

Peptide was reconstituted in 0.5 M TEAB and processed according to the

manufacturer's protocol for TMT kit/iTRAQ kit.

The tryptic peptides were fractionated into fractions by high pH reverse-phase HPLC

using Thermo Betasil C18 column (5 μm particles, 4.6 mm ID, 250 mm length). After

dissolving in the mobile phase A of liquid chromatography, the EASY-nLC 1000

ultra-high performance liquid system is used for separation. Mobile phase A is an

aqueous solution containing 0.1% formic acid and 2% acetonitrile; mobile phase B is

an aqueous solution containing 0.1% formic acid and 90% acetonitrile. Liquid

gradient setting: 0-38 min, 8%~23%B; 38-52 min, 23%~35%B; 52-56 min,

35%~80%B; 56-60 min, 80%B, The flow rate is maintained at 600.00nL min^{-1}. The

peptides are separated by the ultra-high performance liquid system and injected into

the NSI ion source for ionization and then analyzed by QE+1 mass spectrometry. The

ion source voltage was set to 2.2 kV, and the peptide precursor ions and their

secondary fragments were detected and analyzed by high-resolution Orbitrap.

2.8 Mass spectrometry quality control testing

Most of the peptides are distributed in 7-20 amino acids, in line with the general rules

based on trypsin enzymatic hydrolysis and HCD fragmentation. Among them,

peptides with less than 5 amino acids produce too few fragment ions and cannot

produce effective sequence identification. Peptides with more than 20 amino acids are not suitable for HCD fragmentation due to their high mass and charge. The distribution of peptide lengths identified by mass spectrometry meets the quality control requirements(Supplementary Figure S3).

2.9 Quantifification of Calcium Deposition

Cells grown on 6-well plates were washed three with PBS pH 7.4 and decalcified with 0.6 mol L^{-1} HCl for 24 h at 37°C. After decalcification, cells were washed three times with PBS and solubilized with a solution of NaOH 0.1 mol L^{-1} and SDS 0.1% for 30 min, and the protein content of samples was measured with bicinchoninic acid (BCA) protein assay kit (Beyotime Biotechnology, Cat.#P0012, China). The calcium content of the cells was normalized to protein content and expressed as μg/mg protein. The calcium content of the supernatants was determined by the QuantiChrom Calcium Assay Kit (Beyotime Biotechnology, Cat.#S1063S, China).

2.10 ALP activity assay

Cells grown on 6-well plates were washed three with PBS pH 7.4 and 150ul of P0013J (no phosphatase inhibitor) lysis solution was added to each well of cells for 30min on ice. After lysing cells, the alkaline phosphatase (ALP) activity were determined using the ALP assay kit (Beyotime Biotechnology, Cat.#P0321, China), and the protein content of samples was measured with bicinchoninic acid (BCA) protein assay kit. The calcium content of the cells was normalized to protein content and expressed as μg/mg protein.

2.11 Alizarin Red Staining

Cells were washed with phosphate-buffffered saline (PBS) pH (7.2-7.4) and fixed

with 4% paraformaldehyde for 30 min at 37°C. Then, cells were rinsed with PBS and

stained with 1% Alizarin Red S (PH = 4.2）(Solarbio, Cat.#G1452, China) for 5 min.

The Alizarin Red S was discarded and washed 5 times with PBS until the Alizarin

Red S was washed away. The culture plate was placed under the microscope and

observed. Once micrographs were captured, calcium deposits were destained and

dissolved in 10% acetic acid. Absorbance at 420 nm was measured using a multi-

detection microplate reader (Dynex, Lincoln, UK) to quantify calcifification.

2.12 Von Kossa Staining

Cells were washed with phosphate-buffffered saline (PBS) pH (7.2-7.4) and fixed

with 4% paraformaldehyde for 30 min at 37°C, then washed with PBS times and

incubated with reagent A of Von Kossa staining Kit (Solarbio, Cat.#G1452, China)

and placed under ultraviolet light until calcium phosphate turned black. The dye was

washed with PBS three times to remove the excessive dye. Treat with sodium

thiosulfate for two minutes, it was washed three times with PBS. The cell nuclei were

counterstained with Eosin staining solution(Solarbio, Cat.#G1120). Finally, The

culture plate was placed under the microscope and observed.

2.13 Western Blot Analysis

Rats aortic tissue and VSMCs were lysed with ice-cold IP lysis buffer (Thermo Fisher

Scientific) supplemented with complete protease and phosphatase inhibitor cocktail (Thermo

Fisher Scientific). After centrifugation at 12000 rpm for 10 min, the proteins were boiled in

Roti-Load1 Buffer (Carl Roth GmbH) at 100ºC for 10 min. Equal amounts of proteins were

separated on SDS-polyacrylamide gels and transferred to PVDF membranes. The membranes

were incubated overnight at 4°C with primary antibodies: Anti-Mouse IgG(H+L), (diluted

1:5000, A23910, Abbkine), Anti-Rabbit IgG(H+L), (diluted 1:5000, A23920, Abbkine),

Monoclonal Mouse anti-BMP-2/4 (diluted 1:600, SC-137087, Santa Cruz

Biotechnology), Monoclonal Mouse anti-Runx2 (diluted 1:600, SC-101145, Santa Cruz

Biotechnology), Polyclonal Rabbit anti-β-Actin (diluted 1:2000, K101527P, Solarbio),

Monoclonal Rabbit anti-TRAF6(diluted 1:5000, ab40675, Abcam), Monoclonal Mouse

anti-NF-κB p65 (diluted 1:500, #6956, Cell Signaling Technology) and then with

secondary anti-mouse IgG(H+L), (diluted 1:5000, A23910, Abbkine) or anti-rabbit

IgG(H+L), (diluted 1:5000, A23920, Abbkine) for 1 hour at RT. For loading controls, the

membranes were stripped in stripping buffer (Thermo Fisher Scientific) at RT for 40 min.

Antibody binding was detected with Odyssey CLX two-color infrared laser imaging system

(LI-COR). Bands were quantified by using ImageJ software and the results are shown as the

ratio of total protein to β-actin and nuclear protein to Lamin A normalized to the control

groups.

2.14 Quantitative Real-Time RT-PCR

Total RNA was isolated from VSMCs and Rat tissues with RNA Simple Total RNA

Kit（Tiangen Biochemical Technology (Beijing) Co., Ltd. Cat.#DP419, China）

according to the manufacturer's instructions. Reverse transcription of total RNA was

performed using ReverTra Ace qPCR RT Kit（ToYoBo Life Science, Cat.#FSQ-101,

China）. RT-qPCR was performed with the Piko Real-Time PCR Detection System

(Thermo Scientific, Cat.#N11471) and Quantitect SYBR Green Realtime PCR Master

Mix（ToYoBo Life Science，Cat.#QPK-201）according to the manufacturer's

instructions. The primer sequence are shown in Supplementary Table 1.

The specificity of the PCR products was confirmed by analysis of the melting

curves. All PCRs were performed in duplicate, and relative mRNA fold changes were

calculated by the $2^{-\Delta\Delta Ct}$ method using GAPDH as internal reference.

2.15 Statistical analysis

All experiments were independently repeated at least three times. Data are expressed

as the mean ± standard deviation (SD). GraphPad Prism 7.0 was used to analyse the

data and draw figures. Multiple group data were analysed by one−way ANOVA. The

level $P < 0.05$ was considered to indicate a statistically significant difference.

3 RESULTS

3.1 Lanthanum hydroxide delays the development of renal failure and protects renal function

The CKD rat modeling method is shown in Fig.1. In order to evaluate the protective

effect of lanthanum hydroxide on the kidneys of CKD rats, we measured the levels of

serum phosphorus, calcium, creatinine, and urea nitrogen at 4 and 8 weeks after

treatment. As shown in Fig. 2, compared with the control group, the serum

phosphorus, creatinine, and urea nitrogen of the model group increased by 4.85±0.50,

0.31±0.05, 11.88±0.38, and compared with the normal control group, there were

significant differences ($P< 0.01$), suggesting that adenine combined with 1.2% high-

phosphorus diet was successfully modeled. After 4 weeks of administration of

lanthanum hydroxide, compared with the model group, serum phosphorus, creatinine,

and urea nitrogen levels were significantly reduced. As shown in Fig.3, after 8 weeks

of treatment, it can be seen that the lanthanum hydroxide 0.4g kg^{-1} group has the best

phosphorus-lowering effect, and the levels of serum creatinine (Scr) and serum urea

nitrogen (BUN) also decrease in a dose-dependent manner. There was no statistical

difference in the detection results of serum calcium at 4 and 8 weeks after

administration.

According to the results of HE staining of rat kidney in Fig. 4, compared with the

control group, the degeneration and necrosis of the proximal convoluted tubule

epithelial cells in the renal cortex and the disappearance of the nucleus can be

observed in the other groups. The mesenchyme is accompanied by a large number of

mononuclear cell infiltration, glomerular necrosis and disappearance, and visible

protein casts and obvious expansion of the renal tubules. The pathological changes in

the model group were more significant. Chronic granulomatous inflammation was

observed. Purine deposits were seen in some renal tubules. At the same time, there

were also white blood cell casts and renal mesenchymal fibrous tissue focal

hyperplastic lesions in the renal tubules. (Fig. 4B-G). The pathological results of the

lanthanum hydroxide (04g kg^{-1}, 0.2g kg^{-1}, 0.1g kg^{-1}) group showed that compared with the model group, cell deformation and infiltration were lighter, and the degree of renal tubule expansion was significantly improved. Renal interstitial hyperplasia is also effectively controlled, and the glomerular structure is relatively complete. In summary, lanthanum hydroxide can significantly reduce serum phosphorus levels, protect the kidneys, and slow down the development of renal failure.

3.2 Lanthanum hydroxide inhibits the development of vascular calcification

The above results show that lanthanum hydroxide can effectively reduce serum phosphorus levels and defer the progression of renal failure. Because the increase in blood phosphorus is closely related to vascular calcification, we detected serum PTH, and FGF23 levels, and performed computed tomography (CT) examination of rat thoracic aorta and Von Kossa staining of tissue sections.

Compared with the Control group, the serum PTH and FGF23 of the CKD model group were significantly increased. After treatment with lanthanum hydroxide, the serum PTH and FGF23 levels decreased, and compared with the model group, there was a significant difference ($P<0.01$) (Fig. 2E-F; Fig. 3E-F). It can be seen that elevated blood phosphorus can lead to increased levels of PTH and FGF23, the latter being a major regulator of serum phosphorus synthesized and released by osteoblasts, which plays a role in vitamin D metabolism and secondary hyperparathyroidism. It also plays a key role and is directly involved in vascular calcification. Lanthanum hydroxide can slow down the occurrence of vascular calcification by reducing serum phosphorus, thereby reducing the levels of PTH and FGF23 in the serum.

Thoracic aorta slices, stained by Von Kossa, and EVG, are shown in Fig. 5. There was no evidence of vascular calcification in the thoracic section of the aorta among mice in the control groups (Fig. 5a). In contrast, in the model groups, there was clear evidence (positive Von Kossa) of MAC exclusively in the media. Notably, elastin layers in these calcified areas grossly appeared to be disorganized and disrupted (Fig. 5B-b). After 0.4 g kg^{-1} lanthanum hydroxide treatment, a significant reduction in calcification can be observed. And the degree of elastic fiber breakage has also been improved. Calcification of the aorta was evident on computed tomography (CT) imaging of model rat (Fig5C-a, yellow arrows), with the aorta among rat in 0.4% lanthanum hydroxide group being decreased (Fig. 5C-b).

3.3 The proteomic analysis of aortic tissue after Lanthanum hydroxide treatment i*n Vivo*

In order to further explore the mechanism of lanthanum hydroxide delaying the occurrence of vascular calcification, we analyzed the effect of lanthanum hydroxide on the CKD rat model through quantitative proteomics technology, and investigated the expression changes of lanthanum hydroxide on the differential protein in order to verify the relevant signal pathways provide evidence.

Study the differences in aortic proteomics between the Control group and the CKD rat model group, we used TMT labeling, high performance liquid chromatography fractionation technology and mass spectrometry-based quantitative proteomics technology. When P-value<0.05, the change of differential expression exceeding 1.3 is regarded as the change threshold of significant up-regulation, and

less than 1/1.3 is the change threshold of significant down-regulation. The differential

protein quantitative volcano chart is shown (Fig. 6A). The horizontal axis in the figure

is the value of the relative quantitative value of protein after Log2 conversion, and the

vertical axis is the value of the difference significance test P-value after the logarithm

conversion of -Log10. The red points in the figure indicate significantly differentially

expressed up-regulated proteins, and blue points indicate significantly down-regulated

proteins. It can be seen that compared with the Control group, 448 proteins in the

CKD model were significantly up-regulated and 406 proteins were significantly

down-regulated; compared with the CKD model group, 69 proteins were significantly

up-regulated after lanthanum hydroxide administration, 168 Both proteins were

significantly down-regulated.

For biological or technical replicate samples, it is necessary to test whether the

quantitative results of biological or technical replicate samples are statistically

consistent. We conducted two analysis methods, principal component analysis and

Pearson correlation, to evaluate the repeatability of protein quantification. PCA

analysis shows that the Control, Model, and lanthanum hydroxide (0.4g kg^{-1}) groups

have good repeatability and can be completely separated (Fig. 6B); Pearson

correlation analysis also shows that the data has a good linear correlation (Fig. 6C).

In summary, the CKD rat model induced by adenine combined with 1.2% high-

phosphorus diet was successful, and the treatment of lanthanum hydroxide also had a

certain effect on the model rats.

In order to detect whether the differential protein has a significant enrichment

trend in certain functional types, we performed KEGG pathway enrichment analysis

on all differential proteins identified in the screening. For the p-value obtained by the

enrichment test, the bubble chart method showed the pathway of significant

enrichment of differentially modified proteins ($P<0.05$). In Fig. 6 D-E, the vertical

axis is the function classification or pathway, and the horizontal axis is the value after

Log2 conversion of the ratio of the differentially modified protein in the functional

type compared to the ratio of the identified protein. The color of the circle indicates

the enrichment significance P-value, and the size of the circle indicates the number of

differential proteins in the pathway. According to the kegg pathway enrichment

analysis of the Control, Model, and lanthanum hydroxide (0.4g kg^{-1}) groups, It can be

enriched into the nuclear factor-κB (NF-κB) pathway, PI3K-AKT signaling pathways

and cardiovascular Disease-related pathways.

After enriching the differentially modified proteins in different comparison

groups, we performed KEGG cluster analysis on them, aiming to find the correlation

of the differentially modified protein functions after lanthanum hydroxide treatment.

According to the enrichment test P value obtained by the enrichment analysis, the

related functions in different groups are gathered together and drawn into a heat map

using a hierarchical clustering method. The horizontal direction of the heat map

represents different comparison groups, and the vertical direction is the description of

the related functions of differential modification enrichment. Different color blocks

indicate the degree of enrichment, red represents strong enrichment, and blue

represents weak enrichment. Compared with the Model group, the differentially

modified proteins were enriched in the NF-κB signaling pathway after lanthanum hydroxide administration.

The high incidence of cardiovascular disease and mortality in CKD patients is largely caused by medial vascular calcification. Therefore, controlling the occurrence and development of vascular calcification is the key to the prognosis of CKD patients. Vascular calcification is considered to be an active process, mainly regulated by vascular smooth muscle cells. VSMCs can change their phenotype and release stromal vesicles under pathological conditions, which in turn triggers the occurrence of aortic calcification. The phenotypic transdifferentiation of VSMCs is regulated by complex signaling pathways, which are related to systemic inflammation and at least partly depend on the transcription factor NF-κB, which has become a key regulator of vascular calcification. Jakob Voelkl et al. showed that Zinc can inhibit the activation of the NF-κB signal pathway through GPR39-dependent TNFAIP3, thereby inhibiting phosphate-induced osteoblast-like cell transdifferentiation of VSMCs and slowing the development of vascular calcification(Voelkl et al, 2018).

In summary, through a summary of relevant literature and proteomic analysis of aortic tissue, it can be determined that the NF-κB signaling pathway can be used to study the mechanism of lanthanum hydroxide on vascular calcification caused by chronic renal failure hyperphosphatemia .

3.4 Lanthanum hydroxide inhibits Phosphate-Induced Calcification of VSMCs through Suppression of NF- κB *in vitro*.

To determine the promotion in calcifification was due to the reduction in cell viability, the effects of LaCl₃ on cytotoxicity were investigated with an MTT assay. As shown in Supplementary Figure S1, it is determined that the low, medium and high doses of LaCl₃ are divided into 15, 30 and 60uM, and the incubation time is 48h. LaCl₃ has been shown to treat chronic renal failure and hyperphosphatemia. To examine whether LaCl₃ inhibits Pi-provoked mineralization of VSMCs through suppression of NF- κB in our experimental conditions, we cultured VSMCs in calcification medium containing 3 mM inorganic Pi in the presence (15–60 μM) or absence of LaCl₃ and in the presence (1 ug mL⁻¹) or absence of Lipopolysaccharide (LPS) for 6 days. Granular deposits were examined by Alizarin Red Staining and Von Kossa Staining which revealed that Pi significantly promoted mineral deposition compared to the untreated cells, about a 2-fold increase. While the exposure of VSMCs to LaCl₃ dose-dependently decreased Pi-induced mineralization. Importantly, 60 μM LaCl₃ decreased mineral deposition of VSMCs exposed to high Pi down to the level of cells maintained in growth medium (Fig. 7A-B). While the exposure of VSMCs to LaCl₃ dose-dependently decreased calcium deposition and Alkaline phosphatase (ALP) activity, and the inhibition rate reached about 2/3 (Fig. 7C-D). After adding LPS, compared with the high-dose LaCl₃ group, the calcium deposition and ALP activity of the LPS group increased significantly, the calcium deposition almost reached the mid-dose level of LaCl₃. In addition, there were no significant differences in calcium content and ALP activity between the control group and the 60 uM LaCl₃ group (without inorganic Pi) or between the model group and the NaCl group, indicating

that Cl⁻ had no effect on calcification and lanthanum played its role. Overall, these data demonstrate that LaCl₃ effectively inhibits Pi-induced mineral deposition through suppression of NF- κB by human VSMCs in a dose-dependent manner.

3.5 Effects of Lanthanum hydroxide Supplementation on vascular calcification during Chronic Renal Failure *in vivo* and *in vitro*.

To explore the role of lanthanum hydroxide in inhibiting calcification, we initially turned to a robust cell culture-based -3 mM inorganic Pi-induced Western blot and Real-time PCR assay in the VSMCs. The results showed that, compared with the control group, after high Pi induced VSMCs, the expression of smooth muscle SM (SM22α) at gene and protein levels was significantly down-regulated, and the osteogenic markers bone morphogenetic protein 2 (BMP-2) and runt-related transcription factor 2 (Runx2) were significantly up-regulated(Fig. 8A-D, Fig. 8E). Therefore, it can be proved that VSMCs have undergone osteogenic transdifferentiation. In order to verify whether lanthanum chloride regulates the occurrence of vascular calcification through the NF- κB pathway, we detected the protein expression of TNF receptor associated factor 6 (TRAF6) and NF- κB. The results showed that compared with the control group, the expression of TRAF6 and nuclear NF- κB was significantly increased, and when exposed to LaCl₃, its expression was concentration-dependently decreased, compared with the model group. After using the NF-κB agonist LPS, compared with the LaCl₃ (60uM), there is an increasing trend, but not significant(Fig. 8A-D). Because LaCl₃ inhibits the activation of the NF-κB pathway, the expression of SM22α is increased, and the

expression of Runx2 and BMP-2 is decreased, thereby preventing the occurrence of VSMCs mineralization. At the same time, we also performed Western blot and Realtime PCR detection of the aorta of CKD rats. The expression of TRAF6, nuclear NF-κB, BMP-2, and Runx2 was increased in the established CRF model. After 8 weeks of continuous Lanthanum hydroxide treatment, the protein levels of TRAF6, nuclear NF-κB, BMP-2 and Runx2 decreased in a dose-dependent manner in each group(Fig. 9A-D, Fig. 9E). In addition, we detected nuclear translocation of NF-κB by immunofluorescence. As shown in Supplementary Figure S2, under high phosphorus conditions, nuclear translocation of NF-κB occurred, and after giving LaCl$_3$ (60uM), the amount of NF-κB into nucleus was significantly reduced.The results are basically consistent with the results of *in vitro* studies.

In summary, lanthanum hydroxide can inhibit the activation of NF-κB, reduce the expression of osteogenic markers, and thereby inhibit the occurrence of calcification.

4 DISCUSSION

Lanthanum Hydroxide, a new phosphate binder, delayed the progression of kidney failure, suppressed the development of vascular calcification; decreased serum PTH and FGF23 levels; and significantly suppressed serum serum phosphorus. Thus, Lanthanum Hydroxide inhibited the progression of vascular calcification by decreasing serum phosphorus levels.

Various animal models have been developed to investigate MAC formation associated with CKD. Adenine becomes a significant substrate for xanthine

dehydrogenase which oxidizes adenine into 2,8-dihydroxyadenine. 2,8-dihydroxyadenine has a very low solubility and is precipitated in kidney tubules as stones, resulting in nephrolithiasis with extensive tubular dilation, necrosis, and fibrosis, accompanied by renal dysfunction(Tamagaki et al,2006; Tamura M, Aizawa R, Hori M, & Ozaki H, 2009). The adenine model has the advantage of inducing renal failure, with very little variation between animal, over a short period of time(Tamagaki et al, 2006; Massy, ZA, Slama, M, Tribouilloy, C, & Drüeke, TB, 2007).We induced CKD model by adenine combined with 1.2% high-phosphorus diet , the resulting weight loss and increase in levels of BUN and Cre in the CKD rat being comparable to previously reported values. Our results also aligned with a previous report by Jia et al. of an increase in PTH and FGF-23 rose with a prolonged administration of an adenine-containing diet(Jia et al,2013). In the later stages of CKD animal models, bone abnormalities and vascular calcification can be observed in CKD model. Studies in humans demonstrate that abnormal biochemical changes begin when GFR is around 40-50 ml min^{-1} (CKD 3-4), whereas bone and vascular calcification disorders are more prevalent with CKD stages 4-5D(Block et al, 2005; Mehrotra R, & Adler S, 2005; Russo et al, 2007; Levin et al 2007).Taken together, this model allows a characterization of the progressive onset and course of Chronic renal failure.

In this study, Lanthanum hydroxide shows a good therapeutic effect in the rat model of hyperphosphatemia renal failure. By detecting physiological and biochemical indicators, the level of serum phosphorus was improved compared with the model group, and its phosphorus-lowering effect was reduced in a dose-dependent

manner after treatment of lanthanum hydroxide. 0.2g kg^{-1} lanthanum hydroxide treatment decreased serum phosphorus, PTH, FGF23 levels and delays the development of renal failure. The same improvements were observed in the 0.3g kg^{-1} lanthanum carbonate and 0.42g kg^{-1} Calcium carbonate treatments. These results indicated that lanthanum hydroxide had a similar effect to that of the existing drugs. However, 0.4g kg^{-1} lanthanum hydroxide is better than lanthanum carbonate and calcium carbonate, which can achieve better therapeutic effects. In conclusion, the therapeutic advantage of lanthanum hydroxide in the renal failure model of hyperphosphatemia rats was determined.

FGF-23 is secreted by bone cells and osteoblasts. Its main target organs are kidneys and parathyroid glands. It is an important factor that regulates calcium and phosphorus metabolism discovered in recent years. Mirza et al found that higher serum FGF23 levels, even within the normal range, are independently associated with impaired vasoreactivity and increased arterial stiffness in the community(Mirza et al,2009). CKD patients with high FGF-23 are more likely to have impaired vascular reactivity and vascular calcification than patients with normal glomerular filtration rate. Desjardins et al(Desjardins et al, 2012) demonstrsted that elevated levels of FGF-23 were positively correlated with arterial calcification index. In this study, compared with the control group, the FGF23 level in the model group increased to 94.55 mmol mL^{-1}, and treatment with 0.4g kg^{-1} lanthanum hydroxide after 8 weeks, the serum FGF23 decreased to 79.10 mmol mL^{-1} (Fig3-F). Meanwhile, the Von Kossa staining and CT imaging of thoracic aorta in rats after 8 weeks of treatment showed that the

calcification of 0.4 g kg^{-1} lanthanum hydroxide group was significantly reduced

compared with the model group (Fig5). In cultured VSMCs, treatment with LaCl$_3$

blunted phosphate-induced mineral deposition. Granular deposits were examined by

Alizarin Red Staining and Von Kossa Staining which revealed that Pi significantly

promoted mineral deposition compared to the untreated cells, about a 2-fold increase.

While the exposure of VSMCs to LaCl$_3$ dose-dependently decreased Pi-induced

mineralization. Importantly, 60 μM LaCl$_3$ decreased mineral deposition of VSMCs

exposed to high Pi down to the level of cells maintained in growth medium(Fig7).

Therefore, *in vitro* and *in vivo* studies have shown that lanthanum hydroxide can

inhibit the occurrence and development of vascular calcification.

The mechanisms promoting the initiation and progression of vascular

calcification show similarities to those accomplishing physiological bone formation

involving osteo-/chondrogenic transdifferentiation as well as apoptosis of vascular

cells, decreased availability of calcification inhibitors, extracellular vesicle release,

and remodeling of extracellular matrix(Shanahan CM, Crouthamel MH, Kapustin A, &

Giachelli CM, 2011; Alves RD, Eijken M, van de Peppel J, & van Leeuwen JP, 2014; Schlieper

G, Schurgers L, Brandenburg V, Reutelingsperger C, & Floege J, 2016). These mechanisms

are not mutually exclusive. VSMCs play a key role during vascular

calcification(Desjardins et al, 2012; Lanzer et al, 2014; Voelkl et al, 2019). In response to

high extracellular phosphate levels, VSMCs are able to change their phenotype into

osteo-/chondroblast-like cells actively promoting vascular mineralization(Voelkl et al,

2019; Luong et al,2018; Alesutan et al, 2017). These transdifferentiated VSMCs lose their

con-tractile phenotype in favor of a more mesenchymal one and gain similar properties as osteoblasts and chondroblasts(Demer LL, & Tintut Y, 2008). In these vascular smooth muscle cells, the expression of smooth muscle-specific proteins such as α-smooth muscle actin (αSMA) or smooth muscle SM22α is reduced(Steitz et al, 2007). The expression of osteogenic transcription factors such as core-binding factor

α-1 (CBFA1) , homeobox 2 (MSX2) are increased. The transcription factor CBFA1 (also known as Runx2) plays a decisive role in vascular calcification. The osteo-/chondrogenic transcription factors further induce the expression of osteogenic- and chondrogenic-specific proteins in VSMCs such as osteocalcin, type I collagen, BMP-2, or ALP(Lanzer et al, 2014; Voelkl et al, 2019; Leibrock et al, 2016) . Therefore, the osteo-/chondrogenic transdifferentiated VSMCs may promote the calcification of vascular tissue by producing a local pro-calcifying environment and nidus sites for precipitation of calcium and phosphate as well as growth of calcium phosphate crystals. However, so far, the complex processes leading to vascular calcification in CKD remain incompletely understood.

In this study, to investigate the mechanism of lanthanum hydroxide delaying vascular calcification, the thoracic aorta and VSMCs of rats were Western Blotting detected, and the results showed that the SM22α of the model group decreased significantly and the BMP-2 increased significantly compared with the control group, which indicated that VSMCs were transformed into osteoblasts. Subsequently, we identify NF-κB as a key regulator of VSMCs phenotype and calcification. We

demonstrate that Lanthanum supplementation provides powerful protective effects during vascular calcification in vitro and in animal models. High phosphate levels are correlated with vascular calcification, whereas Lanthanum supplementation ameliorates the osteo-/chondrogenic transdifferentiation in VSMCs. The inhibitory effect of Lanthanum inhibits TRAF6 expression, which subsequently inhibits NF-κB activation and osteo-/chondrogenic reprogramming in VSMCs during hyperphosphatemia . However, how La^{3+} enters the cytoplasm, activates the NF-κB pathway, and then mediates the calcification of vascular smooth muscle cells, which will be a direction of our future research(Figure 10).

In conclusion, our study demonstrated that a new type of phosphorus binder-lanthanum hydroxide can effectively reduce serum phosphorus levels, delay the process of renal failure, and protect renal function. Moreover, lanthanum hydroxide can delay the occurrence and development of vascular calcification. This effect is achieved by La^{3+} inhibiting the activation of the NF-κB pathway. Therefore, it lays the foundation of pre-clinical pharmacological research for lanthanum hydroxide to become a clinical candidate drug.

(the Guide for the Care and Use of Laboratory Animals published by the National Institutes of Health; NIH Publication No. 85-23, revised 1996).

CONFLICT OF INTERESTS

The authors declare no competing interests.

DECLARATION OF TRANSPARENCY AND SCIENTIFIC RIGOUR

This Declaration acknowledges that this paper adheres to the principles for transparent reporting and scientific rigor of preclinical research as stated in the BJP guidelines for Design & Analysis, Immunoblotting and Immunochemistry, and Animal Experimentation, and as recommended by funding agencies, publishers, and other organizations engaged with supporting research.

DATA AND MATERIALS AVAILABILITY

The data that support the findings of this study are available from the corresponding author upon reasonable request. Some data may not be made available because of privacy or ethical restrictions.

ORCID

Lu-Lu Zhao, https://orcid.org/0000-0001-8570-2359

Sheng-Nan Wang, https://orcid.org/0000-0003-4071-0544

REFERENCES

Inker LA, Astor BC, Fox CH, Isakova T, Lash JP, Peralta CA, et al. (2014). KDOQI US commentary on the 2012 KDIGO clinical practice guideline for the evaluation and management of CKD. American journal of kidney diseases : the official journal of the National Kidney

Foundation 63: 713–735. https://doi.org/10.1053/j.ajkd.2014.01.416

Mills KT, Xu Y, Zhang W, Bundy JD, Chen CS, Kelly TN, et al. (2015). A systematic analysis of worldwide population-based data on the global burden of chronic kidney disease in 2010. Kidney international 88: 950–957. https://doi.org/10.1038/ki.2015.230

Collins AJ, Foley RN, Gilbertson DT, & Chen SC. (2015). United States Renal Data System public health surveillance of chronic kidney disease and end-stage renal disease. Kidney international supplements 5: 2–7. https://doi.org/10.1038/kisup.2015.2

Masakane I, Nakai S, Ogata S, Kimata N, Hanafusa N, Hamano T,et al. (2015). An Overview of Regular Dialysis Treatment in Japan (As of 31 December 2013). Therapeutic apheresis and dialysis : official peer-reviewed journal of the International Society for Apheresis, the Japanese Society for Apheresis, the Japanese Society for Dialysis Therapy 19: 540–574. https://doi.org/10.1111/1744-9987.12378

Block GA, Klassen PS, Lazarus JM, Ofsthun N, Lowrie EG, & Chertow GM. (2004). Mineral metabolism, mortality, and morbidity in maintenance hemodialysis. Journal of the American Society of Nephrology : JASN 15: 2208–2218. https://doi.org/10.1097/01.ASN.0000133041.27682.A2

Briet M, & Burns KD. (2012). Chronic kidney disease and vascular remodelling: molecular mechanisms and clinical implications. Clinical science (London, England : 1979) 123: 399–416. https://doi.org/10.1042/CS20120074

Smith ER. (2016). Vascular Calcification in Uremia: New-Age Concepts about an Old-Age Problem. Methods in molecular biology (Clifton, N.J.) 1397: 175–208. https://doi.org/10.1007/978-1-4939-3353-2_13

Goodman WG, Goldin J, Kuizon BD, Yoon C, Gales B, Sider D, et al. (2000). Coronary-artery

calcification in young adults with end-stage renal disease who are undergoing dialysis. The New

England journal of medicine 342: 1478–1483. https://doi.org/10.1056/NEJM200005183422003

Russo D, Corrao S, Battaglia Y, Andreucci M, Caiazza A, Carlomagno A, et al. (2011).

Progression of coronary artery calcification and cardiac events in patients with chronic renal

disease not receiving dialysis. Kidney international 80: 112–118.

https://doi.org/10.1038/ki.2011.69

Wang AY, Woo J, Wang M, Sea MM, Ip R, Li PK., et al. (2001). Association of inflammation

and malnutrition with cardiac valve calcification in continuous ambulatory peritoneal dialysis

patients. Journal of the American Society of Nephrology : JASN 12: 1927–1936.

Huveneers S, Daemen MJ, & Hordijk PL. (2015). Between Rho(k) and a hard place: the relation

between vessel wall stiffness, endothelial contractility, and cardiovascular disease. Circulation

research 116: 895–908. https://doi.org/10.1161/CIRCRESAHA.116.305720

London GM, Guérin AP, Marchais SJ., Métivier F, Pannier B, & Adda H. (2003). Arterial media

calcification in end-stage renal disease: impact on all-cause and cardiovascular

mortality. Nephrology, dialysis, transplantation : official publication of the European Dialysis and

Transplant Association - European Renal Association 18: 1731–1740. https://doi.org/10.1093/ndt/
gfg414

Isakova T, Wahl P, Vargas GS, Gutiérrez OM, Scialla J, Xie H, et al. (2011). Fibroblast growth

factor 23 is elevated before parathyroid hormone and phosphate in chronic kidney disease. Kidney

international 79: 1370–1378. https://doi.org/10.1038/ki.2011.47

Tatsumi S, Miyagawa A, Kaneko I, Shiozaki Y, Segawa H, & Miyamoto K. (2016). Regulation of

renal phosphate handling: inter-organ communication in health and disease. Journal of bone and

mineral metabolism 34: 1–10. https://doi.org/10.1007/s00774-015-0705-z

Dhingra R, Sullivan LM., Fox CS., Wang TJ., D'Agostino RB, Sr Gaziano JM, et al. (2007). Relations of serum phosphorus and calcium levels to the incidence of cardiovascular disease in the community. Archives of internal medicine 167: 879–885.

https://doi.org/10.1001/archinte.167.9.879

Da J, Xie X, Wolf M, Disthabanchong S, Wang J, Zha Y, et al. (2015). Serum Phosphorus and Progression of CKD and Mortality: A Meta-analysis of Cohort Studies. American journal of kidney diseases : the official journal of the National Kidney Foundation 66: 258–265.

https://doi.org/10.1053/j.ajkd.2015.01.009

Ma Z, Yu T, Wu Y, Liu D, Zhang X, Miao X, et al. (2019). Nano-lanthanum hydroxide, a novel phosphate binder, for treating hyperphosphatemia: A preclinical study. Biomedicine & pharmacotherapy = Biomedecine & pharmacotherapie 111: 909–916.

https://doi.org/10.1016/j.biopha.2018.12.107

Voelkl J, Tuffaha R, Luong T, Zickler D, Masyout J, Feger M, et al. (2018). Zinc Inhibits Phosphate-Induced Vascular Calcification through TNFAIP3-Mediated Suppression of NF-κB. Journal of the American Society of Nephrology : JASN 29: 1636–1648.

https://doi.org/10.1681/ASN.2017050492

Tamagaki K, Yuan Q, Ohkawa H, Imazeki I. Moriguchi Y, Imai N, et al. (2006). Severe hyperparathyroidism with bone abnormalities and metastatic calcification in rats with adenine-induced uraemia. Nephrology, dialysis, transplantation : official publication of the European Dialysis and Transplant Association - European Renal Association 21: 651–659.

https://doi.org/10.1093/ndt/gfi273

Tamura M, Aizawa R, Hori M, & Ozaki H. (2009). Progressive renal dysfunction and macrophage infiltration in interstitial fibrosis in an adenine-induced tubulointerstitial nephritis mouse

model. Histochemistry and cell biology 131: 483–490. https://doi.org/10.1007/s00418-009-0557-5

Massy, ZA, Slama, M, Tribouilloy, C, & Drüeke, TB. (2007). Animal models--what they can tell us about vascular calcification in CKD. Seminars in dialysis 20: 110–112. https://doi.org/10.1111/j.1525-139X.2007.00256.x

Jia T, Olauson H, Lindberg K, Amin R, Edvardsson K, Lindholm B, et al. (2013). A novel model of adenine-induced tubulointerstitial nephropathy in mice. BMC nephrology 14: 116. https://doi.org/10.1186/1471-2369-14-116

Block GA, Spiegel DM, Ehrlich J, Mehta R, Lindbergh J, Dreisbach A, et al. (2005). Effects of sevelamer and calcium on coronary artery calcification in patients new to hemodialysis. Kidney international 68: 1815–1824. https://doi.org/10.1111/j.1523-1755.2005.00600.x

Mehrotra R, & Adler S. (2005). Coronary artery calcification in nondialyzed patients with chronic kidney diseases. American journal of kidney diseases : the official journal of the National Kidney Foundation 45: 963. https://doi.org/10.1053/j.ajkd.2005.01.041

Russo D, Miranda I, Ruocco C, Battaglia Y, Buonanno E, Manzi S,et al. (2007). The progression of coronary artery calcification in predialysis patients on calcium carbonate or sevelamer. Kidney international 72: 1255–1261. https://doi.org/10.1038/sj.ki.5002518

Levin A, Bakris GL, Molitch M, Smulders M, Tian J, Williams LA,et al. (2007). Prevalence of abnormal serum vitamin D, PTH, calcium, and phosphorus in patients with chronic kidney disease: results of the study to evaluate early kidney disease. Kidney international 71: 31–38. https://doi.org/10.1038/sj.ki.5002009

Mirza MA, Larsson A, Lind L, & Larsson TE. (2009). Circulating fibroblast growth factor-23 is associated with vascular dysfunction in the community. Atherosclerosis 205: 385–390. https://doi.org/10.1016/j.atherosclerosis.2009.01.001

Desjardins L, Liabeuf S, Renard C, Lenglet A, Lemke HD, Choukroun G, et al (2012). FGF23 is independently associated with vascular calcification but not bone mineral density in patients at various CKD stages. Osteoporosis international : a journal established as result of cooperation between the European Foundation for Osteoporosis and the National Osteoporosis Foundation of the USA 23: 2017–2025. https://doi.org/10.1007/s00198-011-1838-0

Shanahan CM, Crouthamel MH, Kapustin A, & Giachelli CM. (2011). Arterial calcification in chronic kidney disease: key roles for calcium and phosphate. Circulation research 109: 697–711. https://doi.org/10.1161/CIRCRESAHA.110.234914

Alves RD, Eijken M, van de Peppel J, & van Leeuwen JP. (2014). Calcifying vascular smooth muscle cells and osteoblasts: independent cell types exhibiting extracellular matrix and biomineralization-related mimicries. BMC genomics 15: 965. https://doi.org/10.1186/1471-2164-15-965

Schlieper G, Schurgers L, Brandenburg V, Reutelingsperger C, & Floege J. (2016). Vascular calcification in chronic kidney disease: an update. Nephrology, dialysis, transplantation : official publication of the European Dialysis and Transplant Association - European Renal Association 31: 31–39. https://doi.org/10.1093/ndt/gfv111

Lanzer P, Boehm M, Sorribas V, Thiriet M, Janzen J, Zeller T, et al. (2014). Medial vascular calcification revisited: review and perspectives. European heart journal 35: 1515–1525. https://doi.org/10.1093/eurheartj/ehu163

Voelkl J, Lang F, Eckardt KU, Amann K, Kuro-O M, Pasch A, et al. (2019). Signaling pathways involved in vascular smooth muscle cell calcification during hyperphosphatemia. Cellular and molecular life sciences : CMLS 76: 2077–2091. https://doi.org/10.1007/s00018-019-03054-z

Luong T, Schelski N, Boehme B, Makridakis M, Vlahou A, Lang F, et al. (2018). Fibulin-3

Attenuates Phosphate-Induced Vascular Smooth Muscle Cell Calcification by Inhibition of

Oxidative Stress. Cellular physiology and biochemistry : international journal of experimental

cellular physiology, biochemistry, and pharmacology 46: 1305–1316.

https://doi.org/10.1159/000489144

Alesutan I, Voelkl J, Feger M, Kratschmar DV, Castor T, Mia S, et al. (2017). Involvement Of

Vascular Aldosterone Synthase In Phosphate-Induced Osteogenic Transformation Of Vascular

Smooth Muscle Cells. Scientific reports 7: 2059. https://doi.org/10.1038/s41598-017-01882-2

Demer LL, & Tintut Y. (2008). Vascular calcification: pathobiology of a multifaceted

disease. Circulation 117: 2938–2948. https://doi.org/10.1161/CIRCULATIONAHA.107.743161

Steitz SA, Speer MY, Curinga G, Yang HY, Haynes P, Aebersold R, et al. (2001). Smooth muscle

cell phenotypic transition associated with calcification: upregulation of Cbfa1 and downregulation

of smooth muscle lineage markers. Circulation research 89: 1147–1154.

https://doi.org/10.1161/hh2401.101070

Leibrock CB, Alesutan I, Voelkl J, Michael D, Castor T, Kohlhofer U, et al. (2016).

Acetazolamide sensitive tissue calcification and aging of klotho-hypomorphic mice. Journal of

molecular medicine (Berlin, Germany), 94(1), 95–106. https://doi.org/10.1007/s00109-015-1331-x
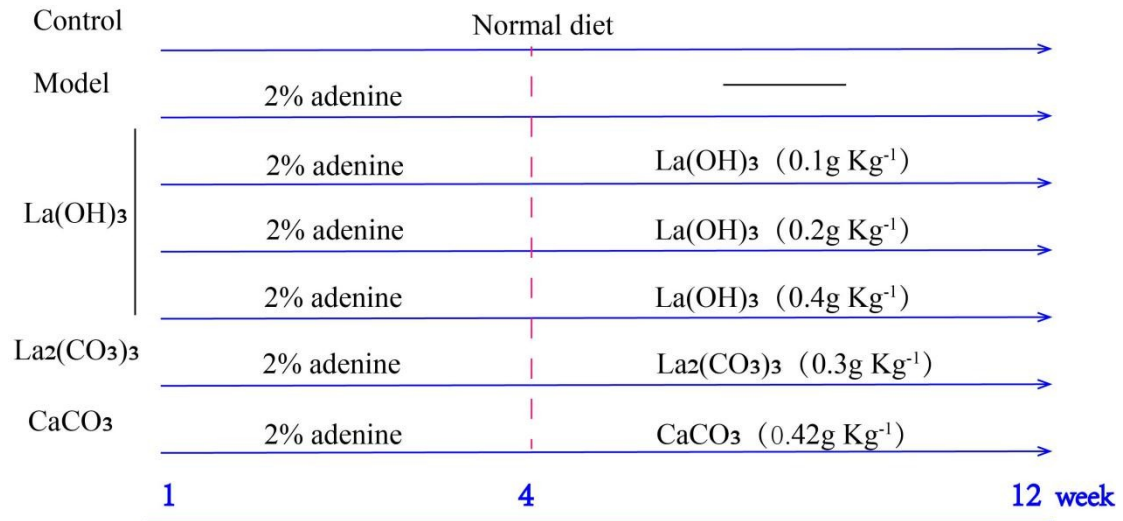
Figure 1. Protocols for the induction of CKD and phosphate loading. Except the control group, all other groups were 1.2% high phosphorus diet for 12 weeks.
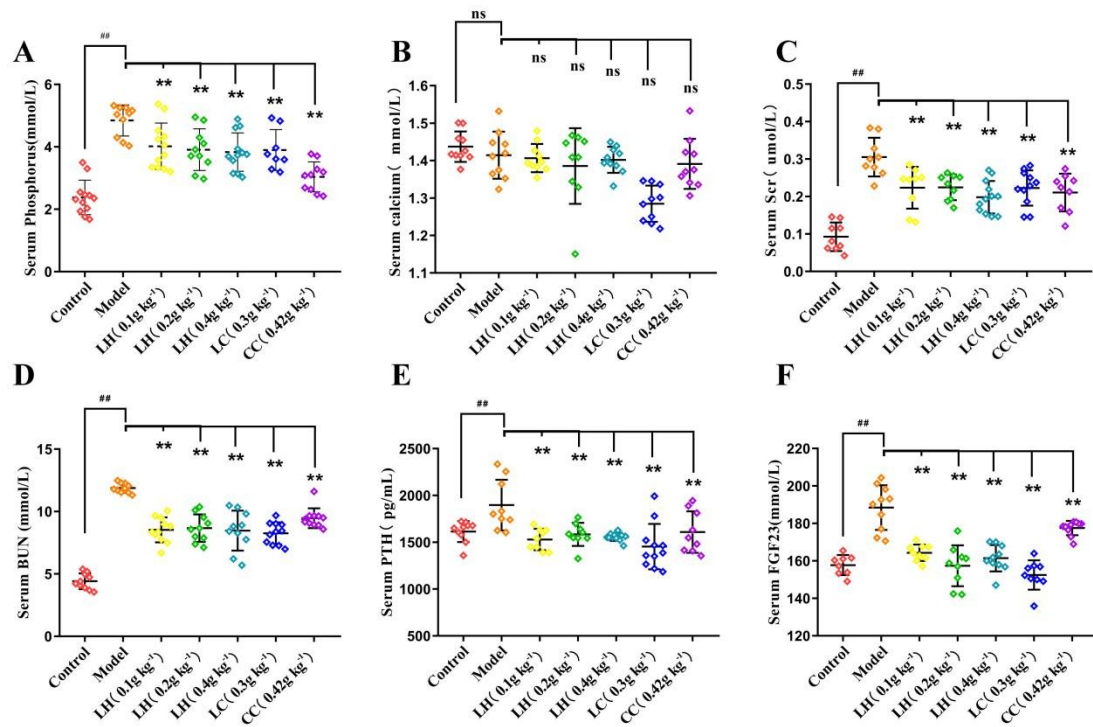
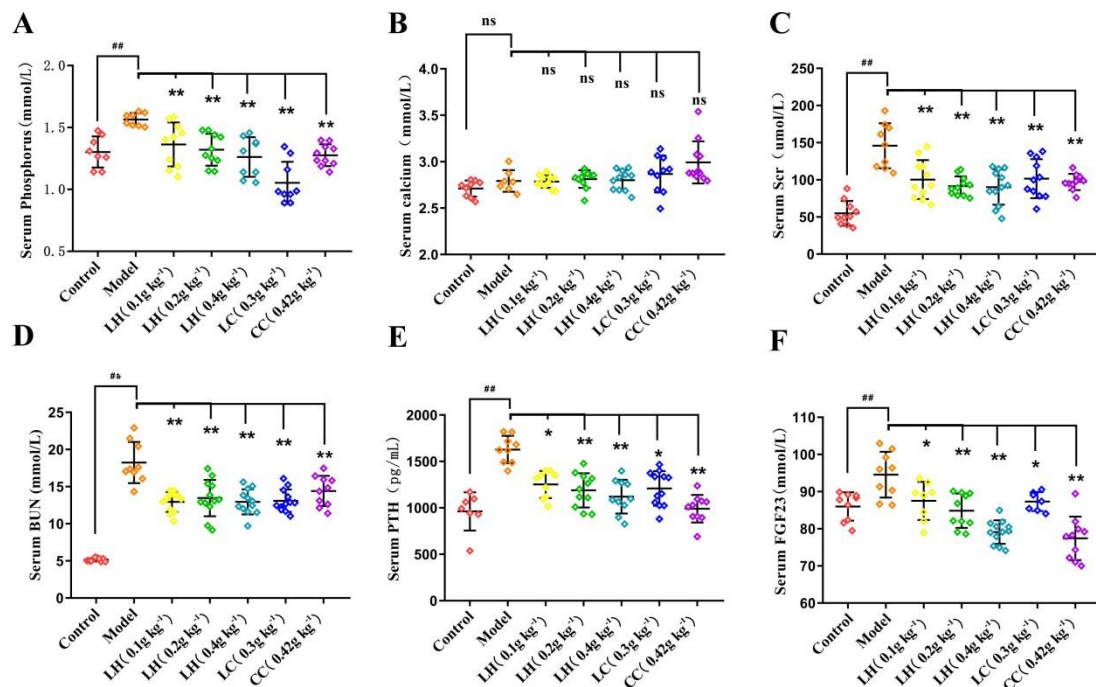**Figure 2. Serum biochemical after lanthanum hydroxide treatment after 4 weeks.**

After 4 weeks of drug treatment, blood was collected from the fundus venous plexus,

and serum biochemistry was tested. A.phosphorus; B.Serum calcium; C. Scr,Serum

creatinine; D. BUN,Serum urea nitrogen; E. PTH,Parathyroid hormone; F.

FGF23,Fibroblast growth factor 23 (mean value ± standard error, $^{\#\#}P < 0.01$

compared with the control ; $^{**}P < 0.01$ compared with the model, NS = not

significant，N=9-11)

Figure 3. Serum biochemical after lanthanum hydroxide treatment after 8 weeks.

After 8 weeks of treatment, blood was collected from the abdominal aorta, and the

serum was collected by centrifugation for serum detection. A. phosphorus; B.Serum

calcium; C. Scr,Serum creatinine; D. BUN,Serum urea nitrogen; E. PTH,Parathyroid

hormone; F. FGF23,Fibroblast growth factor 23 ; (mean value ± standard error, $^{\#\#}P <$

0.01 compared with the control ; $^{**}P < 0.01$ compared with the model, NS = not

significant，*N*=9-11)
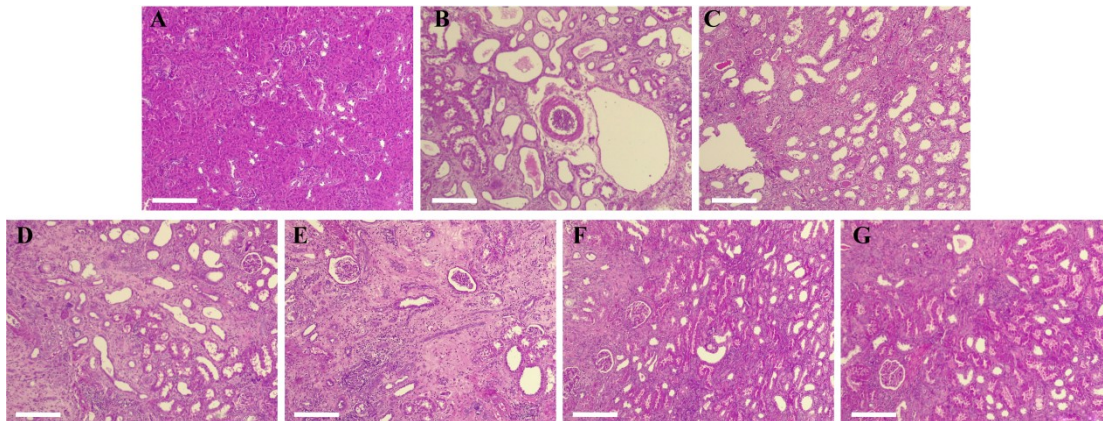
Figure 4. Representative histopathological findings in kidney tissues.

A. control group; B. model group; C. lanthanum hydroxide(0.1g kg^{-1}); D. lanthanum hydroxide(0.2g kg^{-1}); E. lanthanum hydroxide(0.42g kg^{-1}); F. lanthanum carbonate (0.3g kg^{-1}); G. calcium carbonate (0.42 g kg^{-1}). Renal tissue was evaluated in each group using hematoxylin and eosin (H&E) staining. Rat from model groups (4B) exhibited severe tubular impairment, with invasion of inflammatory cells, tubular luminal expansion and fibrotic changes in the stroma. After lanthanum hydroxide treatment, cell deformation and infiltration are lighter, and the degree of renal tubule dilatation is significantly improved(4C-E) . Scale bar =200 μm
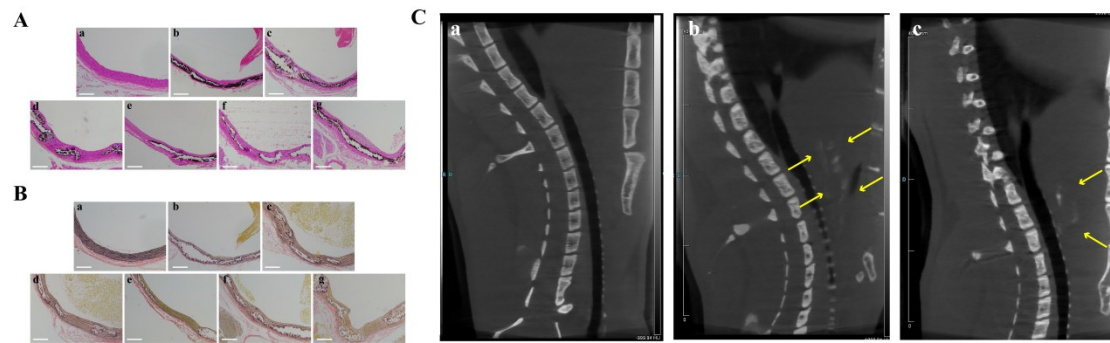
Figure 5. Representative computed tomography (CT) images of ectopic calcification and micrographs of Von Kossa and EVG stained sections of the thracic aorta after 12 weeks.

A. HE stained tissue image of thoracic aorta B. EVG stained tissue image of thoracic aortaa.control group; b. model group; c. lanthanum hydroxide(0.1g kg^{-1}); d. lanthanum hydroxide(0.2g kg^{-1}); e. lanthanum hydroxide(0.4g kg^{-1}); f. lanthanum carbonate (0.3g kg^{-1}); g. calcium carbonate (0.42 g kg^{-1}). Von Kossa and EVG staining positive legions were observed in CKD rat (b.c.d black arrows). Scale bar, 200 μm . C. Positive ectopic calcifications were visible on CT images of model in the thoracic sections of the aorta (C-a.Model group;C-b.lanthanum hydroxide(0.4g kg^{-1}) yellow arrows).
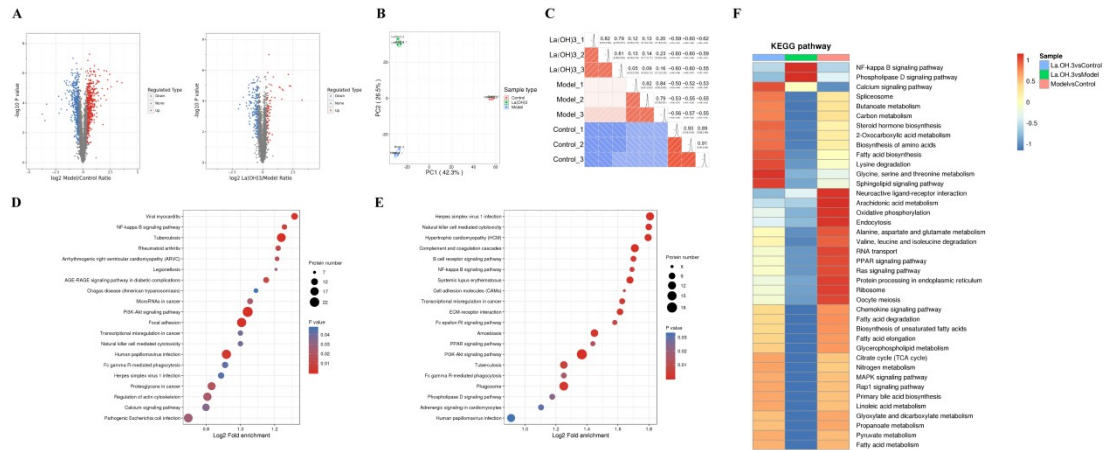
Figure 6. Proteomic analysis of aortic tissue.

A.Differential protein quantitative volcano map. The horizontal axis in the figure is the value of

the relative quantitative value of protein after Log 2 conversion, and the vertical axis is the

value of the difference significance test *P*-value after the logarithm conversion of -Log 10.

The red points in the figure indicate significantly differentially expressed up-regulated

proteins, and blue points indicate significantly down-regulated proteins; **B.** Two-dimensional

scatter plot of protein quantitative principal component analysis among repeated samples. **C.**

Pearson's correlation coefficient heat map ；**D.** KEGG pathway enrichment analysis-Model vs

Control; **E**. KEGG pathway enrichment analysis-La(OH)$_3$ (0.4g kg^{-1}) vs Model; **F.** Cluster

analysis heat map of KEGG pathway. According to the enrichment test P value obtained by the

enrichment analysis, the related functions in different groups are gathered together and drawn

into a heat map using a hierarchical clustering method. The horizontal direction of the heat

map represents different comparison groups, and the vertical direction is the description of the

related functions of differential modification enrichment. Different color blocks indicate the

degree of enrichment, red represents strong enrichment, and blue represents weak enrichment.
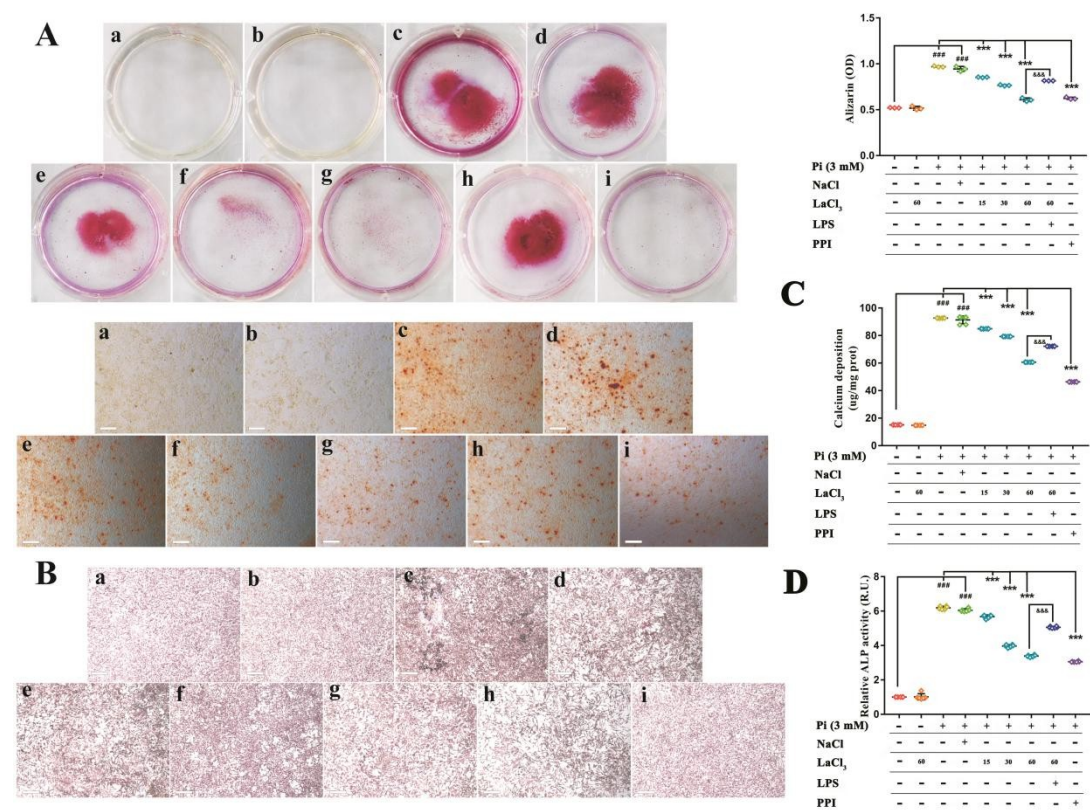
Figure 7. Lanthanum inhibits phosphate induced mineralization of VSMCs in a dose-dependent manner through suppression of NF-κB.

VSMCs were cultured in calcification medium containing 3 mmol/L phosphate (Pi) in the presence (15–60 μM) or absence of lanthanum for 6 days (A–D). (A) Calcium deposition as a marker of mineralization was visualized by Alizarin Red staining. Representative wells and images of stained plates from three independent experiments are shown. Quantification of Alizarin Red to represent the amount of calcium (n=3). (B) Calcium deposition as a marker of mineralization was visualized by Von Kossa Staining. Representative wells and images of stained plates from three independent experiments are shown. (C) Scatter plots and arithmetic means ± SEM (n=6, micrograms per milligram protein) of calcium deposition in VSMCs after treatment for 6 days with control or with Pi, without or with additional treatment with 15-60

uM LaCl₃. (D) Scatter plots and arithmetic means ± SEM (n=6, units per milligram protein) of ALP activity in VSMCs after treatment for 6 days with control or with Pi without or with additional treatment with 15-60 uM LaCl₃. Data are expressed as mean ± SEM of four independent experiments.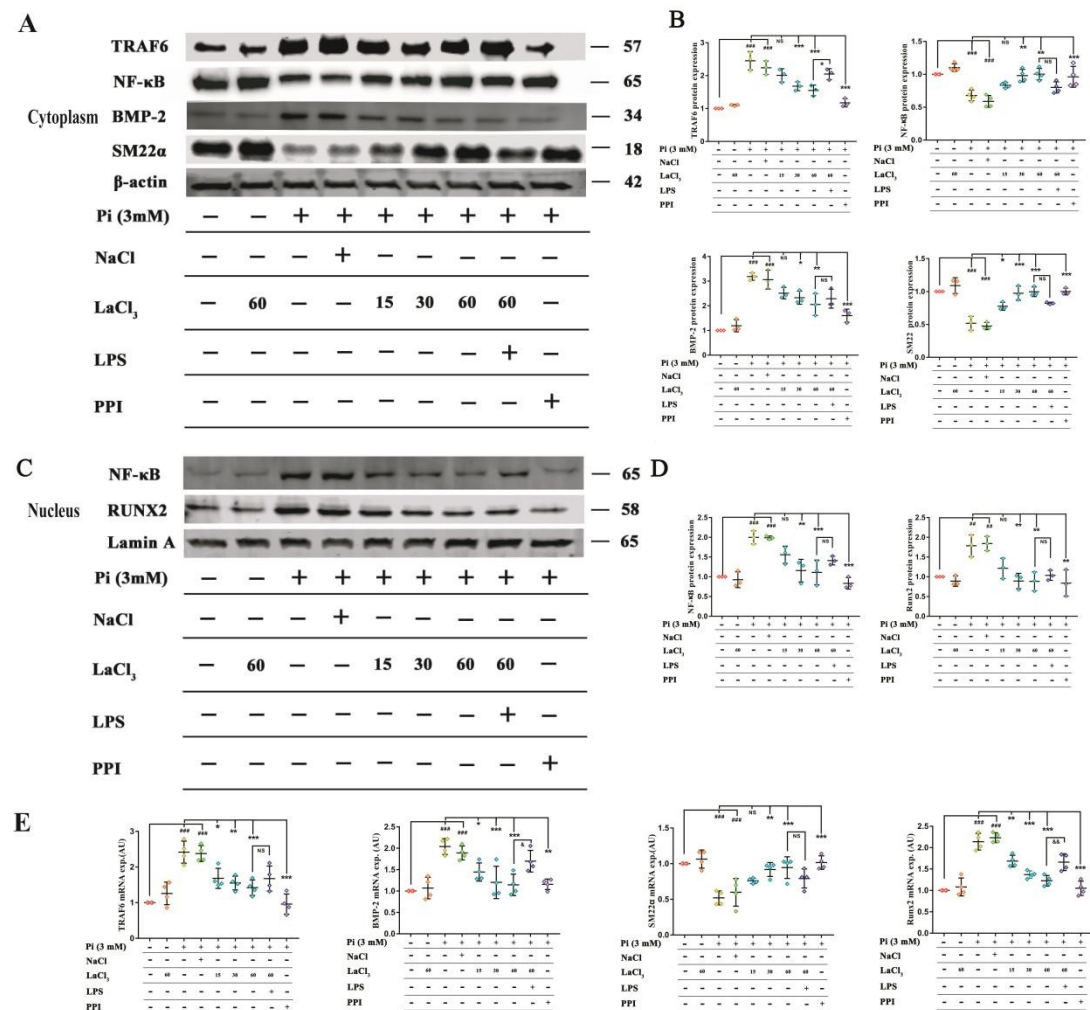 Statistical analysis was performed by one-way ANOVA test. A value of p < 0.05 was considered significant. $^{\#}P < 0.05$; $^{\#\#}P < 0.01$; $^{\#\#\#}P < 0.001$ statistically significant versus control treated VSMCs; $^{*}P < 0.05$; $^{**}P < 0.01$; $^{***}P < 0.001$ statistically significant versus VSMCs treated with Pi alone. $^{\&}P < 0.05$; $^{\&\&}P < 0.01$; $^{\&\&\&}P < 0.001$ statistically significant versus VSMCs treated with Pi and LaCl₃(60 uM). Scale bar =200 μm
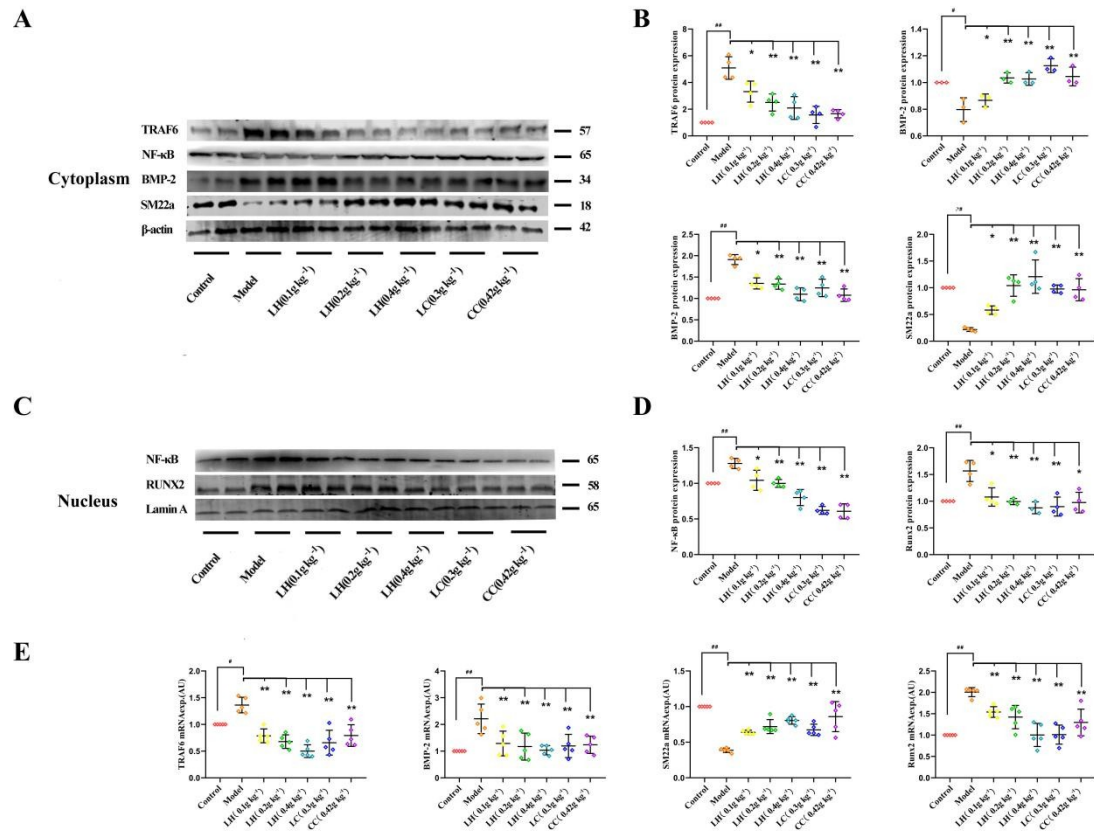
Figure 8. LaCl$_3$ supplementation ameliorates vascular calcification and osteoinductive signaling in chronic renal failure.

(A) Representative original Western blots and Scatter plots and arithmetic means ± SEM (n=3) of normalized cytoplasmic TRAF6/β-actin、NF-κB/β-actin、BMP-2/β-actin and SM22α/β-actin protein ratio in VSMCs with control or with high phosphorus without or with additional treatment with LaCl$_3$. (B) Quantification of Western blots to represent the amount of cytoplasmic protein expression (n=3). (C) Representative original Western blots and Scatter plots and arithmetic means ± SEM (n=3) of normalized nuclear NF-κB/Lamin A and Runx2/Lamin A protein ratio in VSMCs with control or with high phosphorus without or with additional treatment with LaCl$_3$. (D) Quantification of Western blots to represent the amount of nuclear protein expression (n=3). (E) Scatter plots and arithmetic means ± SEM (n=3) of TRAF6, BMP-2, SM22α, and Runx2, relative mRNA expression in VSMCs with control or with high phosphorus without or with additional treatment with LaCl$_3$. [#]*P* < 0.05; [##]*P* < 0.01;[###]*P* < 0.001 statistically significant versus control treated VSMCs; [*]*P* < 0.05; [**]*P* < 0.01; [***]*P* < 0.001 statistically significant versus VSMCs treated with Pi alone. [&]*P* < 0.05; [&&]*P* < 0.01; [&&&]*P* < 0.001 statistically significant versus VSMCs treated with Pi and LaCl$_3$(60 uM).

Figure 9. Lanthanum hydroxide supplementation ameliorates vascular calcification and osteoinductive signaling in chronic renal failure.

(A) Representative original Western blots and Scatter plots and arithmetic means ± SEM (n=3) of normalized cytoplasmic TRAF6/β-actin、NF-κB/β-actin、BMP-2/β-actin and SM22α/β-actin protein ratio in rats with control or with high phosphorus without or with additional treatment with lanthanum hydroxide. (B) Quantification of Western blots to represent the amount of cytoplasmic protein expression (n=3). (C) Representative original Western blots and Scatter plots and arithmetic means ± SEM (n=3) of normalized nuclear NF-κB/Lamin A and Runx2/Lamin A protein ratio in rats with control or with high phosphorus without or with additional treatment with lanthanum hydroxide. (D) Quantification of Western blots to represent the amount of nuclear protein expression (n=3). (E) Scatter plots

and arithmetic means ± SEM (n=3) of TRAF6, BMP-2, SM22α, and Runx2, relative mRNA

expression in rats with control or with high phosphorus without or with additional treatment

with lanthanum hydroxide. #*P* < 0.05; ##*P* < 0.01 statistically significiant versus control

treated rats; *P* < 0.05; **P* < 0.01 statistically significiant versus rats treated with model

group.
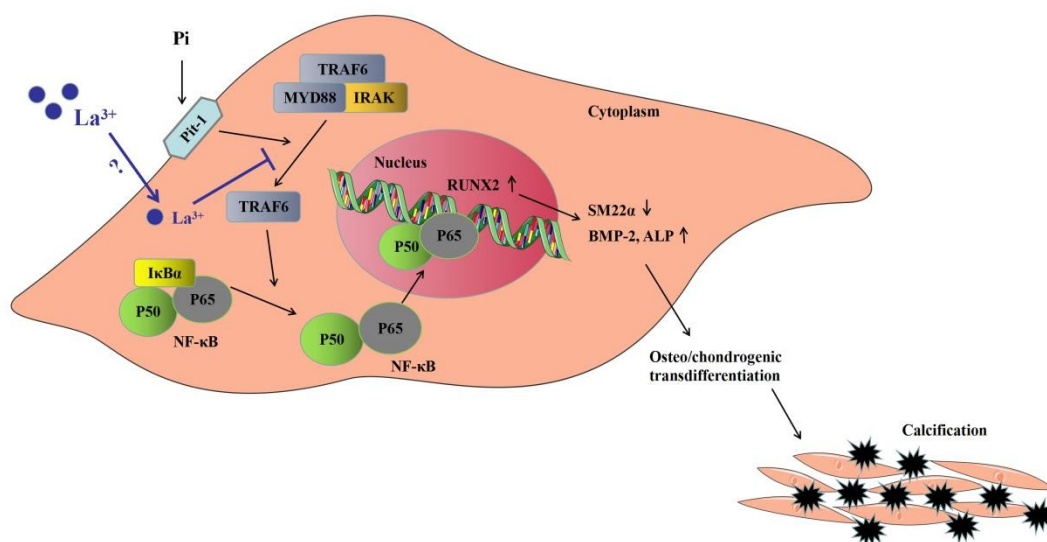
Figure 10. Schematic illustration of phosphate-induced VSMC calcifification and its

inhibition by zinc supplementation.

In VSMCs, exposure to elevated phosphate (Pi) levels induces NF-κB (p50/p65) activation.

NF-κB is activated via phosphorylation-dependent ubiquitination and degradation of IκBα.

The active NF-κB transcription factor translocates to the nucleus and induces target gene

expression to promote osteo-/chondrogenic transdifferentiation of VSMCs. The

osteo-/chondrogenic transdifferentiation of VSMCs induces a procalcifific environment

causing vascular mineralization. Lanthanum supplementation inhibits TRAF6 protein levels. Inhibited TRAF6 protein levels inhibit NF-κB activation, and therefore suppress the osteo-/chondrogenic transdifferentiation of VSMCs, ameliorating the development of a procalcifific environment and subsequent mineralization.

What is already known

- High phosphorus can induce vascular smooth muscle cell transdifferentiation and calcification through NF-κB signaling pathway.

What this study adds

- Lanthanum hydroxide can inhibit the transdifferentiation of VSMCs and calcification by inhibiting the NF-κB signaling pathway.

What is the clinical significance

- The potency of lanthanum hydroxide (0.2g kg^{-1}) is higher than that of lanthanum (0.3g kg^{-1}) carbonate.